# Dense Regular Packings of Irregular Nonconvex Particles
# Supplemental Material

Joost de Graaf,[1,*] René van Roij,[2] and Marjolein Dijkstra[1,†]

[1]*Soft Condensed Matter, Debye Institute for Nanomaterials Science, Utrecht University, Princetonplein 5, 3584 CC Utrecht, The Netherlands*

[2]*Institute for Theoretical Physics, Utrecht University, Leuvenlaan 4, 3584 CE Utrecht, The Netherlands*

(Dated: September 2, 2011)

### Packing Fractions and Crystal Structures for Various Particle Types

In this *Supplemental Material* we present the main body of data we have collected using both our composite technique and literature studies for a large group of solids, particle approximates and several miscellaneous shapes. We also prove that the crystal structures we obtained for rhombicuboctahedra and rhombic enneacontrahedra achieve the densest packing. Furthermore, we present new crystal structures for enneagons, as well as the truncated tetrahedra, which achieve higher packing fractions than previously obtained, both in a centrosymmetric-dimer lattice. In addition to these crystal structures, we consider the relation between the sphericity and packing fraction and show that there is no clear dependence between the two. Finally, we give visual representations for a few of the crystal structures we obtained during our simulation studies.

### Method and Systems

Here, we represent the data gathered by our composite technique of the floppy box Monte Carlo method[1] (FBMC), the triangular tessellation method[2] (TT), and the triangle interference detection method[3] (TID). For the TID routine we implemented the *Robust and Accurate Polygon Interference Detection* library[3] (RAPID). In our simulations we use a modified criterion to perform lattice reduction[4]

$$(1/18) \cdot (|\mathbf{a}| + |\mathbf{b}| + |\mathbf{c}|) \cdot S(\mathbf{a}, \mathbf{b}, \mathbf{c})/V(\mathbf{a}, \mathbf{b}, \mathbf{c}) \;\geq\; 1.5,$$

with $| \cdot |$ the vector norm; $\mathbf{a}$, $\mathbf{b}$, and $\mathbf{c}$ the 3 vectors that span the simulation box; $S(\mathbf{a}, \mathbf{b}, \mathbf{c})$ its surface area; and $V(\mathbf{a}, \mathbf{b}, \mathbf{c})$ its volume.

Systems of tessellated particles were prepared in a dilute phase. By increasing the reduced pressure $p \equiv PV_{\mathrm{M}}/k_{\mathrm{B}}T$ from $p = 1$ to $p \approx 10^5$ over 50,000 Monte Carlo (MC) cycles we compress the system to a high-density crystalline state. Here $P$ is the pressure, $V_{\mathrm{M}}$ is the volume of a particle model, $k_{\mathrm{B}}$ is the Boltzmann constant, $T$ is the temperature, and one cycle is understood to be one trial move per particle. We typically apply this scheme for each number of particles in the unit cell $N$ ($N = 1, \ldots, 6$) and for each considered shape a total of 25 times and select the densest packing among these. These 6 packings (per shape) are allowed to compress for another $10^6$ cycles at $p \approx 10^6$, to obtain a maximally compressed state. Finally, we compare these packings and determine the lowest value of $N$ for which the densest packing is achieved and what the lower bound to the packing fraction of the densest packing $\phi_{\mathrm{LB}}$ is, based on our results.

This way of obtaining densest-packed crystal structures is quite efficient. We find excellent agreement with Refs. [5–9] for the Platonic and Archimedean Solids. That is, the system was typically compressed to within 0.002 of the $\phi_{\mathrm{LB}}$ literature value. The simulations we performed yielded a very narrow distribution of crystal-structure candidates near the closest-packed configuration, typically within 1%. Moreover, the method is quite fast. We observed that in the initial 50,000 MC cycles of compression the algorithm exhibits linear scaling. We disregard the final compression run of $10^6$ MC cycles here, since this part only serves to achieve a high decimal accuracy, while the close packed structure no longer changes. Let $N_T$ be the number of triangles of a specific model, $N_C = 50,000$ the number of MC cycles, and $T$ the total run time of the simulation, we obtained

$$\frac{T}{(NN_C)(NN_T)} = \text{constant}.$$

The algorithm thus scales linearly with the total number of triangles times the total number of attempted moves. The value of this constant differs per model, because some models 'crystallize' more easily than others. For the 159 models we studied, we found that the mean value of this constant is $\sim 70$ $\mu$s with a median value of $\sim 40$ $\mu$s on a modern 2.0 GHz desktop computer system, with only 27 models exceeding 100 $\mu$s. For more information on the TID algorithm and its benchmarking we refer to Ref. [3].

### Tables of Packing Fractions

In Tables I - XI we consider the following quantities: (i) The centrosymmetry of the particle, indicated with 'CS'. 'C' denotes centrosymmetric and 'NC' noncentrosymmetric. (ii) The number of particles $N$ in the unit cell for which densest packing was achieved. (iii) The value of the packing fraction $\phi_{\mathrm{LB}}$ for the densest-known crystal structure. This value has been rounded down to 5 decimals of precision. (iv) The way in which the densest-known packing is accomplished: in a centrosymmetric compound or not. A compound is defined here as an arrangement of particles in space, which are in contact. Our definition is such that the compound may consist of one particle. We abbreviate this parameter by '$\mathrm{CS_c}$', which assumes the values 'y' for yes, 'n' for no, and '-' for packings where we did not verify this property. (v) Similarly, we determine if the densest-known packing admits a space-filling compound, abbreviated with '$\mathrm{SF_c}$', which assumes the analogous values 'Y', 'N', and '-'. (vi) The inscribed-sphere upper bound[7] to the packing fraction $\phi_{\mathrm{UB}}$ that we obtained using constrained optimization. (vii, viii) The outscribed-sphere $\phi_{\mathrm{OS}}$ and oriented-bounding-box $\phi_{\mathrm{OBB}}$ lower bounds to the maximum packing fraction, which were obtained using constrained optimization and the method of Ref. [10]. (ix) The sphericity $\gamma \in [0, 1]$ which we define to be the ratio of the inscribed-sphere radius over the outscribed-sphere radius, in analogy to Ref. [7]. We have supplemented the simulation based material with literature results, since most readers will be predominantly interested in the highest $\phi_{\mathrm{LB}}$ value. We have put references in the footnotes whenever appropriate - only for 29 out of 159 entries a literature result is known.

TABLE I: **Data for the Platonic solids.**

| Code | CS | $N$ | $\phi_{\mathrm{LB}}$ | $\mathrm{CS_c}$ | $\mathrm{SF_c}$ | $\phi_{\mathrm{UB}}$ | $\phi_{\mathrm{OS}}$ | $\phi_{\mathrm{OBB}}$ | $\gamma$ | name |
|---|---|---|---|---|---|---|---|---|---|---|
| PS01 | NC | 4 | 0.85634[a] | y | N | 1.00000 | 0.09072 | 0.33333 | 0.33333 | Tetrahedron |
| PS02 | C | 1 | 0.83635[b] | y | N | 0.89343 | 0.44833 | 0.51502 | 0.79465 | Icosahedron |
| PS03 | C | 1 | 0.90450[b] | y | N | 0.98116 | 0.49235 | 0.47745 | 0.79465 | Dodecahedron |
| PS04 | C | 1 | 0.94736[b] | y | Y[c] | 1.00000 | 0.23570 | 0.56218 | 0.57734 | Octahedron |
| PS05 | C | 1 | 1.00000[b] | y | Y[c] | 1.00000 | 0.27216 | 1.00000 | 0.57734 | Cube |

[a]Ref. [5]

[b]Ref. [6] and [7].

[c]Cubes are space filling.[11,12] Octahedra and tetrahedra form a uniform partition of 3-space (a space-filling compound comprised of Platonic and Archimedean solids) in a 1:2 ratio with equal edge lengths.[11]

[d]The following solids have a nanoparticle or colloid shape equivalent: tetrahedra,[13–15] cubes,[16–18] octahedra,[19,20] dodecahedra (macroscopic),[21] and icosahedra.[15,22,23]

TABLE II: **Data for the Archimedean solids.**

| Code | CS | $N$ | $\phi_{\rm LB}$ | $\rm CS_c$ | $\rm SF_c$ | $\phi_{\rm UB}$ | $\phi_{\rm OS}$ | $\phi_{\rm OBB}$ | $\gamma$ | name |
|---|---|---|---|---|---|---|---|---|---|---|
| AS01 | NC | 2 | $0.99519^a$ | y | $\rm Y^d$ | 1.00000 | 0.29718 | 0.41071 | 0.52223 | Truncated Tetrahedron$^e$ |
| AS02 | C | 1 | $0.78498^b$ | y | N | 0.83856 | 0.64230 | 0.51351 | 0.91495 | Truncated Icosahedron |
| AS03 | NC | 1 | $0.78769^b$ | $\rm n^c$ | N | 0.93492 | 0.57484 | 0.66109 | 0.85033 | Snub Cube$^f$ |
| AS04 | NC | 1 | $0.78864^b$ | $\rm n^c$ | N | 0.85547 | 0.66367 | 0.53018 | 0.91886 | Snub Dodecahedron |
| AS05 | C | 1 | $0.80470^b$ | y | N | 0.83596 | 0.66075 | 0.54747 | 0.92459 | Rhombicosidodecahedron |
| AS06 | C | 1 | $0.82721^b$ | y | N | 0.89731 | 0.66498 | 0.53395 | 0.90494 | Truncated Icosidodecahedron |
| AS07 | C | 1 | $0.84937^b$ | y | N | 1.00000 | 0.59356 | 0.74491 | 0.82594 | Truncated cuboctahedron |
| AS08 | C | 1 | $0.86472^b$ | y | N | 0.93800 | 0.57737 | 0.50464 | 0.85064 | Icosidodecahedron |
| AS09 | C | 1 | $0.87580^b$ | y | N | 0.87580 | 0.56262 | 0.61928 | 0.86285 | Rhombicuboctahedron$^g$ |
| AS10 | C | 1 | $0.89778^b$ | y | N | 0.97387 | 0.57413 | 0.50032 | 0.83850 | Truncated Dodecahedron |
| AS11 | C | 1 | $0.91836^b$ | y | N | 1.00000 | 0.41666 | 0.83333 | 0.70710 | Cuboctahedron |
| AS12 | C | 1 | $0.97374^b$ | y | $\rm Y^d$ | 1.00000 | 0.42712 | 0.96649 | 0.67859 | Truncated Cube |
| AS13 | C | 1 | $1.00000^b$ | y | $\rm Y^d$ | 1.00000 | 0.50596 | 0.53333 | 0.77459 | Truncated Octahedron |

$^a$Ref. [6]
$^b$Ref. [24] and Ref. [25].
$^c$Note that the snub cube and snub dodecahedron are not centrally symmetric, yet they achieve their densest packing in unit cell containing $N = 1$ particles (Bravais lattice), rather than in a non-Bravais lattice, nor do they form a centrosymmetric compound.
$^d$Truncated tetrahedra and tetrahedra from a 2:6 space-filling compound with a 3:1 edge length ratio.[24] Cuboctahedra and octahedra form a 1:1 uniform partition of 3-space with 1:1 edge length ratio.[11] truncated cubes and octahedra form a 1:1 uniform partition of 3-space with edge length ratio 1:1.[11]
$^e$For truncated tetrahedra we obtained a new dimer crystal structure, with $\phi_{\rm LB} = 0.98854\ldots$, which was followed by the discovery of the densest packed dimer lattice.[24,25]
$^f$This result was established using 500 computer experiments for $N = 1, \ldots, 8$ with a slow pressure increase over $4.5 \cdot 10^6$ MC cycles from $p = 1$ to $p = 1.2^{100}$ in 100 steps, followed by $0.5 \cdot 10^6$ MC cycles of production at that pressure. For all systems we approached the literature value $\phi_{\rm LB} = 0.78769\ldots$ to within 0.005 and for each $N$ we obtained the same crystal structure, namely the Bravais lattice of Ref. [6], within the numerical uncertainty of our algorithm.
$^g$We have demonstrated that Rhombicuboctahedra achieve their densest packing in a crystal lattice: $\phi_{\rm LB} = (4/3)(4\sqrt{2} - 5)$.
$^h$The following solids have a nanoparticle or colloid shape equivalent: truncated tetrahedra,[15,26] truncated cubes,[20,26] truncated octahedra,[27] and cuboctahedra.[16,20]

TABLE III: **Data for the Catalan solids.**

| Code | CS | $N$ | $\phi_{\rm LB}$ | $\rm CS_c$ | $\rm SF_c$ | $\phi_{\rm UB}$ | $\phi_{\rm OS}$ | $\phi_{\rm OBB}$ | $\gamma$ | name |
|---|---|---|---|---|---|---|---|---|---|---|
| CS01 | C | 1 | 0.77155 | y | N | 0.78287 | 0.61878 | 0.53980 | 0.92459 | Deltoidal Hexecontahedron |
| CS02 | C | 1 | 0.79693 | y | N | 0.85134 | 0.54691 | 0.54525 | 0.86285 | Deltoidal Icositetrahedron |
| CS03 | C | 1 | 0.79328 | y | N | 0.81365 | 0.45844 | 0.54603 | 0.82594 | Disdyakis Dodecahedron |
| CS04 | C | 1 | 0.76549 | y | N | 0.77313 | 0.57295 | 0.54354 | 0.90494 | Disdyakis Triacontahedron |
| CS05 | NC | 2 | 0.74107 | $\rm n^a$ | N | 0.78283 | 0.60732 | 0.52603 | 0.91886 | Pentagonal Hexecontahedron |
| CS06 | NC | 2 | 0.74363 | $\rm n^a$ | N | 0.84856 | 0.52174 | 0.51407 | 0.85033 | Pentagonal Icositetrahedron |
| CS07 | C | 1 | 0.75755 | y | N | 0.78799 | 0.60356 | 0.53419 | 0.91495 | Pentakis Dodecahedron |
| CS08 | C | 1 | 1.00000 | y | $\rm Y^b$ | 1.00000 | 0.35355 | 0.50000 | 0.70710 | Rhombic Dodecahedron |
| CS09 | C | 1 | 0.80174 | y | N | 0.83462 | 0.51374 | 0.59016 | 0.85064 | Rhombic Triacontahedron |
| CS10 | C | 1 | 0.87601 | y | N | 0.93728 | 0.29289 | 0.63158 | 0.67859 | Small Triakis Octahedron |
| CS11 | C | 1 | 0.81401 | y | N | 0.87841 | 0.40824 | 0.55555 | 0.77459 | Tetrakis Hexahedron |
| CS12 | C | 1 | 0.80479 | y | N | 0.81804 | 0.48227 | 0.55402 | 0.83850 | Triakis Icosahedron |
| CS13 | NC | 2 | 0.79886 | y | N | 1.00000 | 0.16329 | 0.59999 | 0.52223 | Triakis Tetrahedron |

$^a$Note that the pentagonal hexecontahedron and pentagonal icositetrahedron are not centrally symmetric, yet these particles do not achieve their densest-known packing by forming a centrosymmetric compound.
$^b$Rhombic dodecahedra are space filling.[12]
$^c$The following solids have a nanoparticle or colloid shape equivalent: rhombic dodecahedra[17,18] and possibly deltoidal icositetrahedra.[28,29]

TABLE IV: **Data for the Johnson solids**

| Code | CS | $N$ | $\phi_{\mathrm{LB}}$ | $\mathrm{CS_c}$ | $\mathrm{SF_c}$ | $\phi_{\mathrm{UB}}$ | $\phi_{\mathrm{OS}}$ | $\phi_{\mathrm{OBB}}$ | $\gamma$ | name |
|---|---|---|---|---|---|---|---|---|---|---|
| JS01 | NC | 2 | 0.88745 | - | - | 1.00000 | 0.41071 | 0.49624 | 0.73848 | Augmented Dodecahedron |
| JS02 | NC | 2 | 0.97192 | - | - | 1.00000 | 0.21678 | 0.69255 | 0.37819 | Augmented Hexagonal Prism |
| JS03 | NC | 4 | 0.90463 | - | - | 1.00000 | 0.21120 | 0.66082 | 0.42422 | Augmented Pentagonal Prism |
| JS04 | NC | 2 | 0.83264 | - | - | 1.00000 | 0.26330 | 0.44643 | 0.57631 | Augmented Sphenocorona |
| JS05 | NC | 2 | 0.94527 | - | - | 1.00000 | 0.18200 | 0.57321 | 0.48671 | Augmented Triangular Prism |
| JS06 | NC | 2 | 0.85704 | - | - | 1.00000 | 0.13072 | 0.28916 | 0.38646 | Augmented Tridiminished Icosahedron |
| JS07 | NC | 2 | 0.96347 | - | - | 1.00000 | 0.40619 | 0.85433 | 0.63827 | Augmented Truncated Cube |
| JS08 | NC | 1[a] | 0.87969 | - | - | 1.00000 | 0.54646 | 0.51399 | 0.81740 | Augmented Truncated Dodecahedron |
| JS09 | NC | 2 | 0.90795 | - | - | 1.00000 | 0.27695 | 0.57813 | 0.57344 | Augmented Truncated Tetrahedron |
| JS10 | NC | 2 | 0.90677 | - | - | 1.00000 | 0.16543 | 0.56196 | 0.37650 | Biaugmented Pentagonal Prism |
| JS11 | NC | 2 | 0.91501 | - | - | 1.00000 | 0.22322 | 0.60549 | 0.48294 | Biaugmented Triangular Prism |
| JS12 | C | 1 | 0.96102 | y | - | 1.00000 | 0.36374 | 0.78361 | 0.59153 | Biaugmented Truncated Cube |
| JS13 | NC | 2 | 0.81863 | - | - | 1.00000 | 0.62385 | 0.58749 | 0.80687 | Bigyrate Diminished Rhombicosidodecahedron |
| JS14 | C | 1 | 0.95273 | - | - | 1.00000 | 0.19876 | 0.62377 | 0.49112 | Bilunabirotunda |
| JS15 | NC | 2 | 0.82232 | - | - | 1.00000 | 0.62385 | 0.57791 | 0.80687 | Diminished Rhombicosidodecahedron |
| JS16 | NC | 2 | 0.85634 | - | - | 1.00000 | 0.07654 | 0.29003 | 0.33333 | Dipyramid 3 |
| JS17 | NC | 2 | 0.84024 | - | - | 1.00000 | 0.17317 | 0.32759 | 0.49112 | Dipyramid 5 |
| JS18 | NC | 2 | 0.85870 | - | - | 1.00000 | 0.37476 | 0.53256 | 0.69884 | Disphenocingulum |
| JS19 | NC | 2 | 0.83541 | - | - | 1.00000 | 0.36461 | 0.65928 | 0.45045 | Elongated Pentagonal Cupola |
| JS20 | NC | 2 | 0.83751 | - | - | 1.00000 | 0.38059 | 0.46158 | 0.67091 | Elongated Pentagonal Dipyramid |
| JS21 | C | 1 | 0.79475 | y | - | 1.00000 | 0.44920 | 0.60407 | 0.60567 | Elongated Pentagonal Gyrobicupola |
| JS22 | C | 1 | 0.81918 | y | - | 1.00000 | 0.43524 | 0.57603 | 0.74693 | Elongated Pentagonal Gyrobirotunda |
| JS23 | NC | 2 | 0.78374 | - | - | 1.00000 | 0.51299 | 0.58594 | 0.79010 | Elongated Pentagonal Gyrocupolarotunda |
| JS24 | NC | 2 | 0.79329 | - | - | 1.00000 | 0.44920 | 0.60407 | 0.60567 | Elongated Pentagonal Orthobicupola |
| JS25 | NC | 2 | 0.81243 | - | - | 1.00000 | 0.43524 | 0.57603 | 0.74693 | Elongated Pentagonal Orthobirotunda |
| JS26 | NC | 2 | 0.79266 | - | - | 1.00000 | 0.51299 | 0.58594 | 0.79010 | Elongated Pentagonal Orthocupolarotunda |
| JS27 | NC | 2 | 0.86656 | - | - | 1.00000 | 0.35743 | 0.53225 | 0.67555 | Elongated Pentagonal Pyramid |
| JS28 | NC | 2 | 0.81652 | - | - | 1.00000 | 0.44260 | 0.61737 | 0.65993 | Elongated Pentagonal Rotunda |
| JS29 | NC | 2 | 0.85746 | - | - | 1.00000 | 0.43718 | 0.68054 | 0.61012 | Elongated Square Cupola |
| JS30 | C | 1 | 0.90995 | y | - | 1.00000 | 0.14788 | 0.60947 | 0.41421 | Elongated Square Dipyramid |
| JS31 | NC | 2 | 0.80639 | - | - | 0.87580 | 0.56262 | 0.61928 | 0.86285 | Elongated Square Gyrobicupola |
| JS32 | NC | 2 | 0.94371 | - | - | 1.00000 | 0.21844 | 0.72385 | 0.49999 | Elongated Square Pyramid |
| JS33 | NC | 2 | 0.91258 | - | - | 1.00000 | 0.35441 | 0.60017 | 0.65935 | Elongated Triangular Cupola |
| JS34 | NC | 2 | 0.83284 | - | - | 1.00000 | 0.05180 | 0.29326 | 0.21927 | Elongated Triangular Dipyramid |
| JS35 | C | 1 | 0.87941 | y | - | 1.00000 | 0.29486 | 0.62703 | 0.60243 | Elongated Triangular Gyrobicupola |
| JS36 | NC | 2 | 0.88043 | - | - | 1.00000 | 0.29486 | 0.54326 | 0.60243 | Elongated Triangular Orthobicupola |
| JS37 | NC | 4 | 0.86089 | - | - | 1.00000 | 0.09737 | 0.35016 | 0.28867 | Elongated Triangular Pyramid |

[a]Note that the augmented truncated dodecahedron is not centrally symmetric, yet it achieves its densest-known packing for $N = 1$ particles in the unit cell.

TABLE V: **Data for the Johnson solids - continued.**

| Code | CS | $N$ | $\phi_{\mathrm{LB}}$ | $\mathrm{CS_c}$ | $\mathrm{SF_c}$ | $\phi_{\mathrm{UB}}$ | $\phi_{\mathrm{OS}}$ | $\phi_{\mathrm{OBB}}$ | $\gamma$ | name |
|---|---|---|---|---|---|---|---|---|---|---|
| JS38 | NC | 2 | 0.83325 | - | - | 1.00000 | 0.58695 | 0.56431 | 0.77906 | Gyrate Bidiminished Rhombicosidodecahedron |
| JS39 | NC | $1^a$ | 0.80470 | - | - | 0.83596 | 0.66075 | 0.54302 | 0.92459 | Gyrate Rhombicosidodecahedron |
| JS40 | NC | 2 | 1.00000 | - | $\mathrm{Y}^c$ | 1.00000 | 0.15309 | 0.50000 | 0.43301 | Gyrobifastigium |
| JS41 | NC | 2 | 0.76412 | - | - | 1.00000 | 0.42911 | 0.58293 | 0.57146 | Gyroelongated Pentagonal Bicupola |
| JS42 | NC | 2 | 0.77761 | - | - | 0.94171 | 0.45641 | 0.55737 | 0.78549 | Gyroelongated Pentagonal Birotunda |
| JS43 | NC | 4 | 0.80695 | - | - | 1.00000 | 0.34161 | 0.63982 | 0.41448 | Gyroelongated Pentagonal Cupola |
| JS44 | NC | 2 | 0.78540 | - | - | 1.00000 | 0.51719 | 0.56621 | 0.78342 | Gyroelongated Pentagonal Cupolarotunda |
| JS45 | NC | 2 | 0.86077 | - | - | 1.00000 | 0.38637 | 0.50959 | 0.64079 | Gyroelongated Pentagonal Pyramid |
| JS46 | NC | 2 | 0.81250 | - | - | 1.00000 | 0.44203 | 0.59756 | 0.63546 | Gyroelongated Pentagonal Rotunda |
| JS47 | NC | 2 | 0.77850 | - | - | 0.97994 | 0.55378 | 0.54574 | 0.82676 | Gyroelongated Square Bicupola |
| JS48 | NC | 2 | 0.80712 | - | - | 1.00000 | 0.42183 | 0.60324 | 0.56972 | Gyroelongated Square Cupola |
| JS49 | NC | 2 | 0.80261 | - | - | 1.00000 | 0.17614 | 0.43129 | 0.51974 | Gyroelongated Square Dipyramid |
| JS50 | NC | 2 | 0.82236 | - | - | 1.00000 | 0.25752 | 0.45133 | 0.59228 | Gyroelongated Square Pyramid |
| JS51 | NC | 4 | 0.79162 | - | - | 1.00000 | 0.32153 | 0.52112 | 0.67198 | Gyroelongated Triangular Bicupola |
| JS52 | NC | 2 | 0.83145 | - | - | 1.00000 | 0.37306 | 0.56343 | 0.64231 | Gyroelongated Triangular Cupola |
| JS53 | NC | 2 | 0.83853 | - | - | 1.00000 | 0.36444 | 0.54634 | 0.62123 | Hebesphenomegacorona |
| JS54 | NC | 2 | 0.87796 | - | - | 1.00000 | 0.38632 | 0.51502 | 0.71464 | Metabiaugmented Dodecahedron |
| JS55 | NC | 2 | 0.93602 | - | - | 1.00000 | 0.18772 | 0.65039 | 0.35100 | Metabiaugmented Hexagonal Prism |
| JS56 | NC | 2 | 0.86978 | - | - | 1.00000 | 0.53239 | 0.52766 | 0.80327 | Metabiaugmented Truncated Dodecahedron |
| JS57 | NC | 2 | 0.91942 | - | - | 1.00000 | 0.32441 | 0.46065 | 0.57232 | Metabidiminished Icosahedron |
| JS58 | NC | 2 | 0.83373 | - | - | 1.00000 | 0.58695 | 0.56431 | 0.77852 | Metabidiminished Rhombicosidodecahedron |
| JS59 | NC | $1^b$ | 0.80470 | - | - | 0.83596 | 0.66075 | 0.54302 | 0.92459 | Metabigyrate Rhombicosidodecahedron |
| JS60 | NC | $1^b$ | 0.82056 | - | - | 1.00000 | 0.62385 | 0.58749 | 0.80687 | Metagyrate Diminished Rhombicosidodecahedron |
| JS61 | C | 1 | 0.88941 | y | - | 1.00000 | 0.33173 | 0.51502 | 0.67926 | Parabiaugmented Dodecahedron |
| JS62 | C | 1 | 0.97102 | y | - | 1.00000 | 0.13937 | 0.65778 | 0.31783 | Parabiaugmented HexagonalPrism |
| JS63 | C | 1 | 0.88053 | y | - | 1.00000 | 0.51540 | 0.52766 | 0.79465 | Parabiaugmented TruncatedDodecahedron |
| JS64 | C | 1 | 0.85486 | y | - | 1.00000 | 0.58695 | 0.63661 | 0.68915 | Parabidiminished Rhombicosidodecahedron |
| JS65 | C | 1 | 0.80470 | y | - | 0.83596 | 0.66075 | 0.55217 | 0.92459 | Parabigyrate Rhombicosidodecahedron |
| JS66 | NC | $1^a$ | 0.82048 | - | - | 1.00000 | 0.62385 | 0.57791 | 0.80687 | Paragyrate Diminished Rhombicosidodecahedron |
| JS67 | NC | 2 | 0.85648 | - | - | 1.00000 | 0.09698 | 0.44385 | 0.16245 | Pentagonal Cupola |
| JS68 | C | 1 | 0.85891 | y | - | 1.00000 | 0.19397 | 0.44385 | 0.32491 | Pentagonal Gyrobicupola |
| JS69 | NC | 2 | 0.84969 | - | - | 1.00000 | 0.38567 | 0.48784 | 0.58777 | Pentagonal Gyrocupolarotunda |
| JS70 | NC | 2 | 0.82381 | - | - | 1.00000 | 0.19397 | 0.44385 | 0.32491 | Pentagonal Orthobicupola |
| JS71 | NC | 2 | 0.81713 | - | - | 0.93800 | 0.57737 | 0.50464 | 0.85064 | Pentagonal Orthobirotunda |
| JS72 | NC | 2 | 0.83123 | - | - | 1.00000 | 0.38567 | 0.48784 | 0.58777 | Pentagonal Orthocupolarotunda |
| JS73 | NC | 2 | 0.85874 | - | - | 1.00000 | 0.28868 | 0.50464 | 0.42532 | Pentagonal Rotunda |

[a]Note that the gyrate rhombicosidodecahedron and the paragyrate diminished rhombicosidodecahedron are not centrally symmetric, yet they achieve their densest-known packing for $N = 1$ particles in the unit cell. However, both their densest-known $N = 2$ packings form a centrosymmetric-dimer lattice, which achieves a packing fraction remarkably close to that of their $N = 1$ packing.

[b]Note that the metabigyrate rhombicosidodecahedron and metagyrate diminished rhombicosidodecahedron are not centrally symmetric, yet they achieve their densest-known packing in unit cell containing $N = 1$ particles.

[c]The gyrobifastigium is space filling.[12]

TABLE VI: **Data for the Johnson solids - continued.**

| Code | CS | $N$ | $\phi_{\mathrm{LB}}$ | $\mathrm{CS_c}$ | $\mathrm{SF_c}$ | $\phi_{\mathrm{UB}}$ | $\phi_{\mathrm{OS}}$ | $\phi_{\mathrm{OBB}}$ | $\gamma$ | name |
|---|---|---|---|---|---|---|---|---|---|---|
| JS74 | NC | 2 | 0.94582 | - | - | 1.00000 | 0.11785 | 0.33333 | 0.36601 | Pyramid 4 |
| JS75 | NC | 2 | 0.80887 | - | - | 1.00000 | 0.08658 | 0.23032 | 0.27365 | Pyramid 5 |
| JS76 | NC | 2 | 0.86477 | - | - | 1.00000 | 0.18900 | 0.65970 | 0.48676 | Snub Disphenoid |
| JS77 | NC | 4 | 0.81981 | - | - | 1.00000 | 0.34434 | 0.52936 | 0.55150 | Snub Square Antiprism |
| JS78 | NC | 2 | 0.82102 | - | - | 1.00000 | 0.27733 | 0.44893 | 0.58532 | Sphenocorona |
| JS79 | NC | 2 | 0.85093 | - | - | 1.00000 | 0.16304 | 0.39771 | 0.44699 | Sphenomegacorona |
| JS80 | NC | 2 | 0.94227 | - | - | 1.00000 | 0.15397 | 0.47140 | 0.27059 | Square Cupola |
| JS81 | NC | 2 | 0.82692 | - | - | 1.00000 | 0.30795 | 0.47140 | 0.54119 | Square Gyrobicupola |
| JS82 | C | 1 | 0.94249 | y | - | 1.00000 | 0.30795 | 0.55228 | 0.54119 | Square Orthobicupola |
| JS83 | NC | 2 | 0.91836 | - | - | 1.00000 | 0.20833 | 0.41666 | 0.40824 | Triangular Cupola |
| JS84 | NC | 2 | 0.87496 | - | - | 1.00000 | 0.26151 | 0.47213 | 0.49999 | Triangular Hebesphenorotunda |
| JS85 | NC | 2 | 0.88316 | - | - | 1.00000 | 0.41666 | 0.52465 | 0.70710 | Triangular Orthobicupola |
| JS86 | NC | 2 | 0.87421 | - | - | 1.00000 | 0.36090 | 0.52502 | 0.69033 | Triaugmented Dodecahedron |
| JS87 | NC | 2 | 0.89315 | - | - | 1.00000 | 0.15008 | 0.49731 | 0.31783 | Triaugmented Hexagonal Prism |
| JS88 | NC | 2 | 0.82855 | - | - | 1.00000 | 0.20411 | 0.42377 | 0.50211 | Triaugmented Triangular Prism |
| JS89 | NC | 2 | 0.86679 | - | - | 1.00000 | 0.52875 | 0.53355 | 0.79465 | Triaugmented Truncated Dodecahedron |
| JS90 | NC | 2 | 0.91669 | - | - | 1.00000 | 0.26245 | 0.37267 | 0.50209 | Tridiminished Icosahedron |
| JS91 | NC | 2 | 0.84993 | - | - | 1.00000 | 0.55005 | 0.52883 | 0.73251 | Tridiminished Rhombicosidodecahedron |
| JS92 | NC | 2 | 0.80456 | - | - | 0.83596 | 0.66075 | 0.54302 | 0.92459 | Trigyrate Rhombicosidodecahedron |

TABLE VII: **Data for regular prisms.**

| Code | CS | $N$ | $\phi_{\mathrm{LB}}$ | $\mathrm{CS_c}$ | $\mathrm{SF_c}$ | $\phi_{\mathrm{UB}}$ | $\phi_{\mathrm{OS}}$ | $\phi_{\mathrm{OBB}}$ | $\gamma$ | name |
|---|---|---|---|---|---|---|---|---|---|---|
| RP03 | NC | 2 | 1.00000[a] | y | Y[c] | 1.00000 | 0.17181 | 0.50000 | 0.37796 | Prism 3 |
| RP04 | C | 1 | 1.00000[a] | y | Y[c] | 1.00000 | 0.27216 | 1.00000 | 0.57734 | Cube |
| RP05 | NC | 2 | 0.92131[a] | y | N | 1.00000 | 0.31659 | 0.69098 | 0.50673 | Prism 5 |
| RP06 | C | 1 | 1.00000[a] | y | Y[c] | 1.00000 | 0.32863 | 0.75000 | 0.44721 | Prism 6 |
| RP07 | NC | 2 | 0.89269[a] | y | N | 1.00000 | 0.32407 | 0.73825 | 0.39803 | Prism 7 |
| RP08 | C | 1 | 0.90615[a] | y | Y[c] | 1.00000 | 0.31175 | 0.82842 | 0.35740 | Prism 8 |
| RP09 | NC | 2 | 0.90103[b] | y | N | 1.00000 | 0.29629 | 0.75712 | 0.32361 | Prism 9 |
| RP10 | C | 1 | 0.91371[a] | y | N | 1.00000 | 0.28003 | 0.77254 | 0.29524 | Prism 10 |

[a]We used Ref. [30] to compare our results to the literature studies of two-dimensional (2D) regular polygons. See Table I for more information on the cube.
[b]For regular enneaprisms (9-gonal base) we have discovered a new densest packing, which also improves upon the result of Ref. [30] for the regular 9-gon (enneagon, nonagon).
[c]Cubes (square base) and regular tri- (triangular base) and hexaprisms (hexagonal base) are space filling.[11,12] Octaprisms (8-gonal base) can form a space-filling compound with irregular triprisms.

TABLE VIII: **Data for regular antiprisms.**

| Code | CS | $N$ | $\phi_{\mathrm{LB}}$ | $\mathrm{CS_c}$ | $\mathrm{SF_c}$ | $\phi_{\mathrm{UB}}$ | $\phi_{\mathrm{OS}}$ | $\phi_{\mathrm{OBB}}$ | $\gamma$ | name |
|---|---|---|---|---|---|---|---|---|---|---|
| AP03 | C | 1 | 0.94736 | y | Y | 1.00000 | 0.23570 | 0.56218 | 0.57734 | Octahedron[a] |
| AP04 | NC | 2 | 0.86343 | y | N | 1.00000 | 0.30385 | 0.66666 | 0.51108 | Antiprism 4 |
| AP05 | C | 1 | 0.92052 | y | N | 1.00000 | 0.32441 | 0.67418 | 0.44721 | Antiprism 5 |
| AP06 | NC | 2 | 0.88189 | y | N | 1.00000 | 0.32114 | 0.73204 | 0.39331 | Antiprism 6 |
| AP07 | C | 1 | 0.90137 | y | N | 1.00000 | 0.30741 | 0.72740 | 0.34904 | Antiprism 7 |
| AP08 | NC | 2 | 0.89332 | y | N | 1.00000 | 0.28987 | 0.75526 | 0.31270 | Antiprism 8 |
| AP09 | C | 1 | 0.90672 | y | N | 1.00000 | 0.27164 | 0.75000 | 0.28264 | Antiprism 9 |
| AP10 | NC | 2 | 0.89731 | y | N | 1.00000 | 0.25411 | 0.76608 | 0.25750 | Antiprism 10 |

[a]See Table I for more information on the octahedron.

TABLE IX: **Data for several miscellaneous solids.**

| Code | CS | $N$ | $\phi_{\mathrm{LB}}$ | $\mathrm{CS_c}$ | $\mathrm{SF_c}$ | $\phi_{\mathrm{UB}}$ | $\phi_{\mathrm{OS}}$ | $\phi_{\mathrm{OBB}}$ | $\gamma$ | name |
|---|---|---|---|---|---|---|---|---|---|---|
| MS01 | C | 1 | 0.98926 | y | N | 1.00000 | 0.31151 | 0.60300 | 0.59880 | Dürer's Solid[b] |
| MS02 | C | 1 | 1.00000 | y | Y[a] | 1.00000 | 0.31426 | 0.66666 | 0.57734 | Elongated Dodecahedron |
| MS03 | C | 1 | 0.79473 | y | N | 0.79473 | 0.60457 | 0.54914 | 0.91286 | Rhombic Enneacontahedron[c] |
| MS04 | C | 1 | 0.82280 | y | N | 1.00000 | 0.34650 | 0.52786 | 0.64945 | Rhombic Icosahedron |
| MS05 | NC | 2 | 1.00000 | y | Y[a] | 1.00000 | 0.35355 | 0.50000 | 0.70710 | Squashed Dodecahedron |
| MS06 | NC | 4 | 0.70503 | n | N | 1.00000 | 0.13380 | 0.31616 | 0.41221 | Stanford Bunny[d] |
| MS07 | NC | 2 | 0.47242 | y | N | 1.00000 | 0.00853 | 0.06853 | 0.11355 | Hammerhead Shark[d] |

[a]The elongated dodecahedron and the squashed dodecahedron are space filling.
[b]Note that Dürer's Solid is not the same as the dimer compound formed by truncated tetrahedra.
[c]For the rhombic enneacontahedron we have shown that the Bravais lattice we discovered achieves the densest packing.
[d]For the Stanford bunny[31] and the hammerhead shark[32] the number of triangles that comprise these models is very high, 3756 and 5116 triangles respectively, however all quantities could be established with the appropriate accuracy.

TABLE X: **Data for nonconvex polyhedra.**

| Code | CS | $N$ | $\phi_{\mathrm{LB}}$ | $\mathrm{CS_c}$ | $\mathrm{SF_c}$ | $\phi_{\mathrm{UB}}$ | $\phi_{\mathrm{OS}}$ | $\phi_{\mathrm{OBB}}$ | $\gamma$ | name |
|---|---|---|---|---|---|---|---|---|---|---|
| PH01 | NC | 2 | 0.61327 | n | N | 1.00000 | 0.04157 | 0.23149 | 0.17469 | Császár Polyhedron |
| PH02 | C | 1 | 0.29477 | y | N | 1.00000 | 0.07659 | 0.06269 | 0.26640 | Echidnahedron |
| PH03 | C | 1 | 1.00000 | y | Y[a] | 1.00000 | 0.22922 | 0.45845 | 0.55284 | Escher's Solid |
| PH04 | C | 1 | 0.55728 | y | N | 1.00000 | 0.21644 | 0.20989 | 0.51160 | Great Rhombictriacontrahedron |
| PH05 | C | 2 | 0.88967 | n | N | 1.00000 | 0.18806 | 0.18237 | 0.18759 | Great Stellated Dodecahedron |
| PH06 | C | 1 | 0.74965 | y | N | 1.00000 | 0.34558 | 0.39699 | 0.53633 | Jessen's Orthogonal Icosahedron |
| PH07 | C | 1 | 0.55602 | y | N | 1.00000 | 0.20643 | 0.20019 | 0.51455 | Mathematica Spikey 1[b] |
| PH08 | C | 1 | 0.59998 | y | N | 1.00000 | 0.14378 | 0.20246 | 0.35355 | Rhombic Dodecahedron Stellation 2[c] |
| PH09 | C | 2 | 0.55654 | n | N | 1.00000 | 0.19854 | 0.19253 | 0.41946 | Rhombic Hexecontrahedron |
| PH10 | C | 2 | 0.69528 | n | N | 0.97719 | 0.49635 | 0.47293 | 0.79787 | Small Triambic Icosahedron |
| PH11 | NC | 2 | 0.51913 | y | N | 1.00000 | 0.03637 | 0.13732 | 0.16538 | Szilassi Polyhedron |

[a]Escher's solid is space filling by construction.
[b]The number '1' in the name 'Mathematica spikey 1' refers to the first version of the Mathematica spikey, which was used as a logo for the first version of the Mathematica software package.[33] It is a cumulated icosahedron with cumulation ratio $\sqrt{6}/3$.
[c]The number '2' in the name 'rhombic dodecahedron stellation 2' refers to the fact that there are three stellations of the rhombic dodecahedron (four when including the original). This particular stellation is listed as number '2' in the Mathematica polyhedron database.[34]

TABLE XI: **Data for nonconvex nanoparticle and colloid approximates.**

| Code | CS | $N$ | $\phi_{\mathrm{LB}}$ | $\mathrm{CS_c}$ | $\mathrm{SF_c}$ | $\phi_{\mathrm{UB}}$ | $\phi_{\mathrm{OS}}$ | $\phi_{\mathrm{OBB}}$ | $\gamma$ | name |
|---|---|---|---|---|---|---|---|---|---|---|
| PA01 | NC | 4 | 0.51850 | n | N | 1.00000 | 0.18253 | 0.27282 | 0.155754 | Cap[b] |
| PA02 | C | 1 | 0.68615 | y | N | 1.00000 | 0.09602 | 0.22903 | 0.38489 | Nanostar |
| PA03 | C | 1 | 0.31077 | y | N | 1.00000 | 0.02525 | 0.06681 | 0.13281 | Octapod |
| PA04 | NC | 2[a] | 0.59207 | y | N | 1.00000 | 0.04864 | 0.10628 | 0.20303 | Tetrapod |

[a]The tetrapod achieves its densest-known packing for $N = 2$ particles in the unit cell, however, the densest-known $N = 1$ the packing fraction is remarkably close to that value.
[b]The cap[35] is comprised of 3850 triangles. Despite this model's complexity, all quantities could be established with the appropriate accuracy.

**Densest Packing Configurations for Rhombicuboctahedra and Rhombic Enneacontrahedra**

In this section we prove that the densest-packed configurations for rhombicuboctahedra $\phi_{\mathrm{LB}} = (4/3)\left(4\sqrt{2}-5\right)$ and for rhombic enneacontrahedra $\phi_{\mathrm{LB}} = 16 - 34/\sqrt{5}$ are given by their Bravais lattices.

**Rhombicuboctahedron:** Let the rhombicuboctahedron (RCH) be specified by the vertex coordinates

$$\left(i\left(\frac{1}{2}+\frac{p}{\sqrt{2}}\right), j\left(\frac{1}{2}+\frac{q}{\sqrt{2}}\right), k\left(\frac{1}{2}+\frac{r}{\sqrt{2}}\right)\right),$$

where $i$, $j$, and $k \in \{-1,1\}$ and $p$, $q$, and $r \in \{0,1\}$, with $p+q+r=1$. This gives a list of 24 vertices centred on the origin, which span a RCH with volume $4+10\sqrt{2}/3$. For this system a possible choice of three vectors which describe a unit cell that realizes the densest packing, is given by

$$\begin{aligned}
v_0 &= \left(1+\frac{1}{\sqrt{2}}, -1-\frac{1}{\sqrt{2}}, 0\right), \\
v_1 &= \left(1+\frac{1}{\sqrt{2}}, 0, -1-\frac{1}{\sqrt{2}}\right), \\
v_2 &= \left(0, 1+\frac{1}{\sqrt{2}}, 1+\frac{1}{\sqrt{2}}\right).
\end{aligned}$$

Checking for overlaps in this configuration is a simple matter of verifying that there are no overlaps for an appropriate number of nearest neighbors. It follows that the volume of the unit cell is given by $|v_0 \cdot (v_1 \times v_2)| = 5 + 7/\sqrt{2}$. Therefore, the packing fraction is

$$\phi_{\mathrm{LB}} = \frac{4+10\sqrt{2}/3}{5+7/\sqrt{2}} = \frac{4}{3}\left(4\sqrt{2}-5\right).$$

We determined the face-to-point minimum distance for all 26 faces of the RCH, which leads to a set of 26 constrained equations. Using constrained minimization on this set of equations the maximum inscribed sphere can be obtained. Its radius is $1/2 + 1/\sqrt{2}$ and it is centred on the origin. This results in the following upper-bound estimate for the packing fraction

$$\phi_{\mathrm{UB}} = \frac{\pi}{\sqrt{18}} \frac{4+10\sqrt{2}/3}{(4\pi/3)\left(1/2+1/\sqrt{2}\right)^3} = \frac{4}{3}\left(4\sqrt{2}-5\right).$$

We have thus proven that the maximum packing fraction is obtained, since $\phi_{\mathrm{UB}} = \phi_{\mathrm{LB}}$. Here is should be noted that this proof is conditionally dependent on the proof of Ref. [36] via the proof for the upper-bound criterion of Ref. [7].

**Rhombic enneacontrahedron:** Let the rhombic enneacontrahedron (RECH) be described by the 92 vertex coordinates listed in Tables XII and XIII. These are centred on the origin and span a RECH with volume

$$\frac{20}{3}\sqrt{43+\frac{56\sqrt{5}}{3}}.$$

For this system a possible set of three vectors which describes a unit cell that realizes the densest packing, is given by

$$\begin{aligned}
v_0 &= \left(-\frac{5}{6}\left(2+\sqrt{5}\right), \frac{1}{2}\sqrt{\frac{5}{3}}, \frac{1}{3}\left(5+2\sqrt{5}\right)\right), \\
v_1 &= \left(-\frac{5}{12}\left(1+\sqrt{5}\right), \sqrt{\frac{235}{24}+\frac{35\sqrt{5}}{8}}, \frac{1}{6}\left(5+\sqrt{5}\right)\right), \\
v_2 &= \left(\frac{1}{12}\left(25+13\sqrt{5}\right), \frac{5+\sqrt{5}}{4\sqrt{3}}, \frac{1}{6}\left(5+\sqrt{5}\right)\right).
\end{aligned}$$

Checking for overlaps in this configuration is again a simple matter. It follows that the volume of the unit cell is given by

$$|v_0 \cdot (v_1 \times v_2)| = \frac{10\left(20 + 9\sqrt{5}\right)}{3\sqrt{3}}.$$

Therefore, the packing fraction that is achieved for this structure is $\phi_{\mathrm{LB}} = 16 - 34/\sqrt{5}$. By determining the set of 90 face-to-point constrained equations, the maximum inscribed sphere is easily determined to be centred on the origin and have radius

$$\sqrt{\frac{35}{12} + \frac{5\sqrt{5}}{4}},$$

using constrained minimization. This results in the following upper bound to the packing fraction $\phi_{\mathrm{UB}} = 16 - 34/\sqrt{5}$. We have thus proven that the maximum packing is obtained.

TABLE XII: **Vertices of the rhombic enneacontrahedron.**

| | |
|---|---|
| $\left(\frac{1}{3}\left(-5-\sqrt{5}\right), 0, \frac{1}{3}\left(-7+2\sqrt{5}\right)\right)$ | $\left(\frac{1}{3}\left(-5-\sqrt{5}\right), 0, \frac{2}{3}\left(-2+\sqrt{5}\right)\right)$ |
| $\left(\frac{1}{6}\left(-7-3\sqrt{5}\right), -\sqrt{\frac{1}{6}\left(3+\sqrt{5}\right)}, \frac{2}{3}\left(-3+\sqrt{5}\right)\right)$ | $\left(\frac{1}{6}\left(-7-3\sqrt{5}\right), -\sqrt{\frac{1}{6}\left(3+\sqrt{5}\right)}, -1+\frac{2\sqrt{5}}{3}\right)$ |
| $\left(\frac{1}{6}\left(-7-3\sqrt{5}\right), \sqrt{\frac{1}{6}\left(3+\sqrt{5}\right)}, \frac{2}{3}\left(-3+\sqrt{5}\right)\right)$ | $\left(\frac{1}{6}\left(-7-3\sqrt{5}\right), \sqrt{\frac{1}{6}\left(3+\sqrt{5}\right)}, -1+\frac{2\sqrt{5}}{3}\right)$ |
| $\left(-\frac{2}{3}\left(1+\sqrt{5}\right), 0, \frac{2}{3}\left(-1+\sqrt{5}\right)\right)$ | $\left(\frac{1}{3}\left(-4-\sqrt{5}\right), -\frac{1}{\sqrt{3}}, \frac{1}{3}\left(-7+\sqrt{5}\right)\right)$ |
| $\left(\frac{1}{3}\left(-4-\sqrt{5}\right), \frac{1}{\sqrt{3}}, \frac{1}{3}\left(-7+\sqrt{5}\right)\right)$ | $\left(\frac{1}{6}\left(-5-3\sqrt{5}\right), -\sqrt{\frac{7}{6}+\frac{\sqrt{5}}{2}}, \frac{1}{3}\left(-6+\sqrt{5}\right)\right)$ |
| $\left(\frac{1}{6}\left(-5-3\sqrt{5}\right), -\sqrt{\frac{7}{6}+\frac{\sqrt{5}}{2}}, \frac{1}{3}\left(-3+\sqrt{5}\right)\right)$ | $\left(\frac{1}{6}\left(-5-3\sqrt{5}\right), \sqrt{\frac{1}{6}\left(7+3\sqrt{5}\right)}, \frac{1}{3}\left(-6+\sqrt{5}\right)\right)$ |
| $\left(\frac{1}{6}\left(-5-3\sqrt{5}\right), \sqrt{\frac{1}{6}\left(7+3\sqrt{5}\right)}, \frac{1}{3}\left(-3+\sqrt{5}\right)\right)$ | $\left(-1-\frac{\sqrt{5}}{3}, 0, -\frac{7}{3}\right)$ |
| $\left(\frac{1}{2}\left(-1-\sqrt{5}\right), -\sqrt{\frac{1}{6}\left(3+\sqrt{5}\right)}, -2\right)$ | $\left(\frac{1}{2}\left(-1-\sqrt{5}\right), -\sqrt{\frac{1}{6}\left(3+\sqrt{5}\right)}, -1+\sqrt{5}\right)$ |
| $\left(\frac{1}{2}\left(-1-\sqrt{5}\right), \sqrt{\frac{1}{6}\left(3+\sqrt{5}\right)}, -2\right)$ | $\left(\frac{1}{2}\left(-1-\sqrt{5}\right), \sqrt{\frac{1}{6}\left(3+\sqrt{5}\right)}, -1+\sqrt{5}\right)$ |
| $\left(\frac{1}{6}\left(-7-\sqrt{5}\right), -\sqrt{\frac{7}{6}+\frac{\sqrt{5}}{2}}, \frac{2}{3}\left(-1+\sqrt{5}\right)\right)$ | $\left(\frac{1}{6}\left(-7-\sqrt{5}\right), \sqrt{\frac{1}{6}\left(7+3\sqrt{5}\right)}, \frac{2}{3}\left(-1+\sqrt{5}\right)\right)$ |
| $\left(-\frac{2\sqrt{5}}{3}, 0, -\frac{2}{3}+\sqrt{5}\right)$ | $\left(\frac{1}{6}\left(-5-\sqrt{5}\right), -\sqrt{\frac{5}{6}\left(3+\sqrt{5}\right)}, \frac{1}{3}\left(-5+\sqrt{5}\right)\right)$ |
| $\left(\frac{1}{6}\left(-5-\sqrt{5}\right), -\sqrt{\frac{5}{6}\left(3+\sqrt{5}\right)}, \frac{1}{3}\left(-2+\sqrt{5}\right)\right)$ | $\left(\frac{1}{6}\left(-5-\sqrt{5}\right), \sqrt{\frac{5}{6}\left(3+\sqrt{5}\right)}, \frac{1}{3}\left(-5+\sqrt{5}\right)\right)$ |
| $\left(\frac{1}{6}\left(-5-\sqrt{5}\right), \sqrt{\frac{5}{6}\left(3+\sqrt{5}\right)}, \frac{1}{3}\left(-2+\sqrt{5}\right)\right)$ | $\left(\frac{1}{3}\left(-1-\sqrt{5}\right), -\sqrt{\frac{2}{3}\left(3+\sqrt{5}\right)}, \frac{1}{3}\left(-7+\sqrt{5}\right)\right)$ |
| $\left(\frac{1}{3}\left(-1-\sqrt{5}\right), \sqrt{\frac{2}{3}\left(3+\sqrt{5}\right)}, \frac{1}{3}\left(-7+\sqrt{5}\right)\right)$ | $\left(\frac{1}{6}\left(-3-\sqrt{5}\right), -\sqrt{\frac{7}{6}+\frac{\sqrt{5}}{2}}, -\frac{2}{3}+\sqrt{5}\right)$ |
| $\left(\frac{1}{6}\left(-3-\sqrt{5}\right), -\sqrt{\frac{1}{6}\left(3-\sqrt{5}\right)}, -\frac{8}{3}\right)$ | $\left(\frac{1}{6}\left(-3-\sqrt{5}\right), \sqrt{\frac{1}{6}\left(3-\sqrt{5}\right)}, -\frac{8}{3}\right)$ |
| $\left(\frac{1}{6}\left(-3-\sqrt{5}\right), \sqrt{\frac{1}{6}\left(7+3\sqrt{5}\right)}, -\frac{2}{3}+\sqrt{5}\right)$ | $\left(-\frac{\sqrt{5}}{3}, -\sqrt{\frac{5}{3}}, -\frac{7}{3}\right)$ |
| $\left(-\frac{\sqrt{5}}{3}, -\frac{1}{\sqrt{3}}, -\frac{1}{3}+\sqrt{5}\right)$ | $\left(-\frac{\sqrt{5}}{3}, \frac{1}{\sqrt{3}}, -\frac{1}{3}+\sqrt{5}\right)$ |
| $\left(-\frac{\sqrt{5}}{3}, \sqrt{\frac{5}{3}}, -\frac{7}{3}\right)$ | $\left(\frac{1}{6}\left(-1-\sqrt{5}\right), -\sqrt{\frac{5}{6}\left(3+\sqrt{5}\right)}, \frac{2}{3}\left(-1+\sqrt{5}\right)\right)$ |
| $\left(\frac{1}{6}\left(-1-\sqrt{5}\right), \sqrt{\frac{5}{6}\left(3+\sqrt{5}\right)}, \frac{2}{3}\left(-1+\sqrt{5}\right)\right)$ | $\left(-\frac{1}{3}, -\sqrt{3+\frac{4\sqrt{5}}{3}}, \frac{1}{3}\left(-6+\sqrt{5}\right)\right)$ |
| $\left(-\frac{1}{3}, -\sqrt{3+\frac{4\sqrt{5}}{3}}, \frac{1}{3}\left(-3+\sqrt{5}\right)\right)$ | $\left(-\frac{1}{3}, \sqrt{3+\frac{4\sqrt{5}}{3}}, \frac{1}{3}\left(-6+\sqrt{5}\right)\right)$ |

TABLE XIII: **Vertices of the rhombic enneacontrahedron - continued.**

| | |
|---|---|
| $\left(-\frac{1}{3}, \sqrt{3+\frac{4\sqrt{5}}{3}}, \frac{1}{3}\left(-3+\sqrt{5}\right)\right)$ | $\left(\frac{1}{6}\left(-3+\sqrt{5}\right), -\sqrt{\frac{1}{6}\left(3+\sqrt{5}\right)}, -\frac{1}{3}+\sqrt{5}\right)$ |
| $\left(\frac{1}{6}\left(-3+\sqrt{5}\right), \sqrt{\frac{1}{6}\left(3+\sqrt{5}\right)}, -\frac{1}{3}+\sqrt{5}\right)$ | $\left(0, -\sqrt{\frac{2}{3}\left(3+\sqrt{5}\right)}, -2\right)$ |
| $\left(0, -\sqrt{\frac{2}{3}\left(3+\sqrt{5}\right)}, -1+\sqrt{5}\right)$ | $(0, 0, -3)$ |
| $(0, 0, \sqrt{5})$ | $\left(0, \sqrt{\frac{2}{3}\left(3+\sqrt{5}\right)}, -2\right)$ |
| $\left(0, \sqrt{\frac{2}{3}\left(3+\sqrt{5}\right)}, -1+\sqrt{5}\right)$ | $\left(\frac{1}{6}\left(3-\sqrt{5}\right), -\sqrt{\frac{1}{6}\left(3+\sqrt{5}\right)}, -\frac{8}{3}\right)$ |
| $\left(\frac{1}{6}\left(3-\sqrt{5}\right), \sqrt{\frac{1}{6}\left(3+\sqrt{5}\right)}, -\frac{8}{3}\right)$ | $\left(\frac{1}{3}, -\sqrt{3+\frac{4\sqrt{5}}{3}}, \frac{2}{3}\left(-3+\sqrt{5}\right)\right)$ |
| $\left(\frac{1}{3}, -\sqrt{3+\frac{4\sqrt{5}}{3}}, -1+\frac{2\sqrt{5}}{3}\right)$ | $\left(\frac{1}{3}, \sqrt{3+\frac{4\sqrt{5}}{3}}, \frac{2}{3}\left(-3+\sqrt{5}\right)\right)$ |
| $\left(\frac{1}{3}, \sqrt{3+\frac{4\sqrt{5}}{3}}, -1+\frac{2\sqrt{5}}{3}\right)$ | $\left(\frac{1}{6}\left(1+\sqrt{5}\right), -\sqrt{\frac{5}{6}\left(3+\sqrt{5}\right)}, \frac{1}{3}\left(-7+\sqrt{5}\right)\right)$ |
| $\left(\frac{1}{6}\left(1+\sqrt{5}\right), \sqrt{\frac{5}{6}\left(3+\sqrt{5}\right)}, \frac{1}{3}\left(-7+\sqrt{5}\right)\right)$ | $\left(\frac{\sqrt{5}}{3}, -\sqrt{\frac{5}{3}}, -\frac{2}{3}+\sqrt{5}\right)$ |
| $\left(\frac{\sqrt{5}}{3}, -\frac{1}{\sqrt{3}}, -\frac{8}{3}\right)$ | $\left(\frac{\sqrt{5}}{3}, \frac{1}{\sqrt{3}}, -\frac{8}{3}\right)$ |
| $\left(\frac{\sqrt{5}}{3}, \sqrt{\frac{5}{3}}, -\frac{2}{3}+\sqrt{5}\right)$ | $\left(\frac{1}{6}\left(3+\sqrt{5}\right), -\sqrt{\frac{7}{6}+\frac{\sqrt{5}}{2}}, -\frac{7}{3}\right)$ |
| $\left(\frac{1}{6}\left(3+\sqrt{5}\right), -\sqrt{\frac{1}{6}\left(3-\sqrt{5}\right)}, -\frac{1}{3}+\sqrt{5}\right)$ | $\left(\frac{1}{6}\left(3+\sqrt{5}\right), \sqrt{\frac{1}{6}\left(3-\sqrt{5}\right)}, -\frac{1}{3}+\sqrt{5}\right)$ |
| $\left(\frac{1}{6}\left(3+\sqrt{5}\right), \sqrt{\frac{1}{6}\left(7+3\sqrt{5}\right)}, -\frac{7}{3}\right)$ | $\left(\frac{1}{3}\left(1+\sqrt{5}\right), -\sqrt{\frac{2}{3}\left(3+\sqrt{5}\right)}, \frac{2}{3}\left(-1+\sqrt{5}\right)\right)$ |
| $\left(\frac{1}{3}\left(1+\sqrt{5}\right), \sqrt{\frac{2}{3}\left(3+\sqrt{5}\right)}, \frac{2}{3}\left(-1+\sqrt{5}\right)\right)$ | $\left(\frac{1}{6}\left(5+\sqrt{5}\right), -\sqrt{\frac{5}{6}\left(3+\sqrt{5}\right)}, \frac{1}{3}\left(-7+2\sqrt{5}\right)\right)$ |
| $\left(\frac{1}{6}\left(5+\sqrt{5}\right), -\sqrt{\frac{5}{6}\left(3+\sqrt{5}\right)}, \frac{2}{3}\left(-2+\sqrt{5}\right)\right)$ | $\left(\frac{1}{6}\left(5+\sqrt{5}\right), \sqrt{\frac{5}{6}\left(3+\sqrt{5}\right)}, \frac{1}{3}\left(-7+2\sqrt{5}\right)\right)$ |
| $\left(\frac{1}{6}\left(5+\sqrt{5}\right), \sqrt{\frac{5}{6}\left(3+\sqrt{5}\right)}, \frac{2}{3}\left(-2+\sqrt{5}\right)\right)$ | $\left(\frac{2\sqrt{5}}{3}, 0, -\frac{7}{3}\right)$ |
| $\left(\frac{1}{6}\left(7+\sqrt{5}\right), -\sqrt{\frac{7}{6}+\frac{\sqrt{5}}{2}}, \frac{1}{3}\left(-7+\sqrt{5}\right)\right)$ | $\left(\frac{1}{6}\left(7+\sqrt{5}\right), \sqrt{\frac{1}{6}\left(7+3\sqrt{5}\right)}, \frac{1}{3}\left(-7+\sqrt{5}\right)\right)$ |
| $\left(\frac{1}{2}\left(1+\sqrt{5}\right), -\sqrt{\frac{1}{6}\left(3+\sqrt{5}\right)}, -2\right)$ | $\left(\frac{1}{2}\left(1+\sqrt{5}\right), -\sqrt{\frac{1}{6}\left(3+\sqrt{5}\right)}, -1+\sqrt{5}\right)$ |
| $\left(\frac{1}{2}\left(1+\sqrt{5}\right), \sqrt{\frac{1}{6}\left(3+\sqrt{5}\right)}, -2\right)$ | $\left(\frac{1}{2}\left(1+\sqrt{5}\right), \sqrt{\frac{1}{6}\left(3+\sqrt{5}\right)}, -1+\sqrt{5}\right)$ |
| $\left(\frac{1}{3}\left(3+\sqrt{5}\right), 0, -\frac{2}{3}+\sqrt{5}\right)$ | $\left(\frac{1}{6}\left(5+3\sqrt{5}\right), -\sqrt{\frac{7}{6}+\frac{\sqrt{5}}{2}}, \frac{2}{3}\left(-3+\sqrt{5}\right)\right)$ |
| $\left(\frac{1}{6}\left(5+3\sqrt{5}\right), -\sqrt{\frac{7}{6}+\frac{\sqrt{5}}{2}}, -1+\frac{2\sqrt{5}}{3}\right)$ | $\left(\frac{1}{6}\left(5+3\sqrt{5}\right), \sqrt{\frac{1}{6}\left(7+3\sqrt{5}\right)}, \frac{2}{3}\left(-3+\sqrt{5}\right)\right)$ |
| $\left(\frac{1}{6}\left(5+3\sqrt{5}\right), \sqrt{\frac{1}{6}\left(7+3\sqrt{5}\right)}, -1+\frac{2\sqrt{5}}{3}\right)$ | $\left(\frac{1}{3}\left(4+\sqrt{5}\right), -\frac{1}{\sqrt{3}}, \frac{2}{3}\left(-1+\sqrt{5}\right)\right)$ |
| $\left(\frac{1}{3}\left(4+\sqrt{5}\right), \frac{1}{\sqrt{3}}, \frac{2}{3}\left(-1+\sqrt{5}\right)\right)$ | $\left(\frac{2}{3}\left(1+\sqrt{5}\right), 0, \frac{1}{3}\left(-7+\sqrt{5}\right)\right)$ |
| $\left(\frac{1}{6}\left(7+3\sqrt{5}\right), -\sqrt{\frac{1}{6}\left(3+\sqrt{5}\right)}, \frac{1}{3}\left(-6+\sqrt{5}\right)\right)$ | $\left(\frac{1}{6}\left(7+3\sqrt{5}\right), -\sqrt{\frac{1}{6}\left(3+\sqrt{5}\right)}, \frac{1}{3}\left(-3+\sqrt{5}\right)\right)$ |
| $\left(\frac{1}{6}\left(7+3\sqrt{5}\right), \sqrt{\frac{1}{6}\left(3+\sqrt{5}\right)}, \frac{1}{3}\left(-6+\sqrt{5}\right)\right)$ | $\left(\frac{1}{6}\left(7+3\sqrt{5}\right), \sqrt{\frac{1}{6}\left(3+\sqrt{5}\right)}, \frac{1}{3}\left(-3+\sqrt{5}\right)\right)$ |
| $\left(\frac{1}{3}\left(5+\sqrt{5}\right), 0, \frac{1}{3}\left(-5+\sqrt{5}\right)\right)$ | $\left(\frac{1}{3}\left(5+\sqrt{5}\right), 0, \frac{1}{3}\left(-2+\sqrt{5}\right)\right)$ |

**New Crystal Structures for Enneagons and Truncated Tetrahedra**

In this section we describe the construction of a new crystal structure for enneagons (nonagons, regular 9-gon), which achieves the densest-known packing. The method we use here has similarities the ones employed in Refs. [5] and [9]; both of these present the analytic construction of a dense family of tetrahedral dimers. Finally, we list our numerical data, by which the dimer lattice of truncated tetrahedra can be constructed.

**Enneagons:** We begin with some basic definitions. An enneagon is defined here to have a centre-to-tip distance of 1. It is centred on the origin of a Cartesian coordinate system with its tips mirror-symmetrically distributed around the $y$-axis and one tip located on the positive $y$-axis. To describe the crystal structure we further require three two-dimensional (2D) vector parameterizations

$$\begin{aligned}
p_1(q) &= \left(q\left(\sin\left[\frac{\pi}{9}\right]-\frac{\sqrt{3}}{2}\right)+2\cos\left[\frac{\pi}{9}\right]\sin\left[\frac{2\pi}{9}\right], \frac{1}{4}\left(q\left(2-4\cos\left[\frac{\pi}{9}\right]\right)-\csc\left[\frac{\pi}{18}\right]\right)\right),\\
p_2(r) &= \left(2\cos\left[\frac{\pi}{9}\right]\sin\left[\frac{\pi}{9}\right]-r\sin\left[\frac{2\pi}{9}\right], 2\cos^2\left[\frac{\pi}{9}\right]+r\left(1-\cos\left[\frac{2\pi}{9}\right]\right)\right),\\
p_3(s) &= \left(s\left(\sin\left[\frac{\pi}{9}\right]-\frac{\sqrt{3}}{2}\right)+2\cos\left[\frac{\pi}{9}\right]\sin\left[\frac{2\pi}{9}\right], -\frac{1}{4}\left(s\left(2-4\cos\left[\frac{\pi}{9}\right]\right)-\csc\left[\frac{\pi}{18}\right]\right)\right),
\end{aligned}$$

with $q$, $r$, and $s \in [-1, 1]$. We will employ these to describe lattice vectors and positions of the enneagons in the unit cell. We eliminate two of the variables such that different enneagons in the lattice have some of their edges and corners touch and slide over each other upon varying the third:

$$\begin{aligned}
T(k,l) &= \frac{\csc\left[\frac{2\pi}{9}\right]}{4\left(\cos\left[\frac{2\pi}{9}\right]-1\right)}\cdot\\
&\quad \left\{\sqrt{3}\left(\cos\left[\frac{2\pi}{9}\right]-1\right)(k+l)+2\sin\left[\frac{\pi}{9}\right](k+l)-8\sin\left[\frac{\pi}{9}\right]\cos\left[\frac{\pi}{9}\right]\right.\\
&\quad -\sin\left[\frac{\pi}{9}\right]\cos\left[\frac{2\pi}{9}\right](k+l)+8\sin\left[\frac{\pi}{9}\right]\cos\left[\frac{\pi}{9}\right]\cos\left[\frac{2\pi}{9}\right]+\sin\left[\frac{2\pi}{9}\right](l-k)\\
&\quad \left.-2\sin\left[\frac{2\pi}{9}\right]\cos\left[\frac{\pi}{9}\right](l-k)+8\sin\left[\frac{2\pi}{9}\right]\cos\left[\frac{\pi}{9}\right]-8\sin\left[\frac{2\pi}{9}\right]\cos\left[\frac{\pi}{9}\right]\cos\left[\frac{2\pi}{9}\right]\right\}\\
U(k) &= \left\{\sqrt{3}k+2\cos\left[\frac{\pi}{18}\right]-k\cos\left[\frac{\pi}{18}\right]-\sqrt{3}k\cos\left[\frac{\pi}{9}\right]+2k\cos\left[\frac{\pi}{18}\right]\cos\left[\frac{\pi}{9}\right]+\sqrt{3}k\sin\left[\frac{\pi}{18}\right]-k\sin\left[\frac{\pi}{9}\right]\right.\\
&\quad \left.4\sin\left[\frac{\pi}{18}\right]\cos\left[\frac{\pi}{18}\right]-2k\sin\left[\frac{\pi}{18}\right]\sin\left[\frac{\pi}{9}\right]-4\sin\left[\frac{2\pi}{9}\right]\cos\left[\frac{\pi}{9}\right]-8\sin\left[\frac{\pi}{18}\right]\sin\left[\frac{2\pi}{9}\right]\cos\left[\frac{\pi}{9}\right]\right\}\\
V(k) &= \sin\left[\frac{\pi}{9}\right]+2\sin\left[\frac{\pi}{18}\right]\sin\left[\frac{\pi}{9}\right]-\cos\left[\frac{\pi}{18}\right]-\sqrt{3}\left(\sin\left[\frac{\pi}{18}\right]+\cos\left[\frac{\pi}{9}\right]\right)+2\cos\left[\frac{\pi}{18}\right]\cos\left[\frac{\pi}{9}\right]\\
W(k) &= \frac{U(k)}{V(k)},
\end{aligned}$$

with $k$ and $l \in [-1, 1]$. Using $T(k,l)$ and $W(k)$, we may write

$$\begin{aligned}
P_0(k) &= (0,0),\\
P_1(k) &= p_2\left(T\left(k, W\left(k\right)\right)\right),\\
V_0(k) &= p_3\left(W\left(k\right)\right)+p_2\left(T\left(k, W\left(k\right)\right)\right),\\
V_1(k) &= p_1\left(k\right)+p_3\left(W\left(k\right)\right),
\end{aligned}$$

where the $P_i$ give the position of the enneagons in the unit cell ($N = 2$) with lattice vectors $V_i$ ($i \in \{0, 1\}$). The enneagon at $P_0$ has the same orientation as the base enneagon defined above and the one at $P_1$ is rotated by $\pi$ with respect to the base enneagon, also see Fig. 1a which shows this configuration for the densest-known packing. By determining the value of $k$, say $k^*$, for which the volume fraction $F_v$ associated to this lattice is maximized,

$$F_v(k) = \frac{18\sin\left[\frac{\pi}{9}\right]\cos\left[\frac{\pi}{9}\right]}{\left|V_{0,x}(k)V_{1,y}(k)-V_{0,y}(k)V_{1,x}(k)\right|},$$

we obtain the lattice with the highest-known packing fraction. For this value of $k$, we obtain the following

$$\begin{aligned}
k^* &= 0.334782056761309\ldots, \\
F_v(k^*) &= 0.901030078420934\ldots = \phi_{\mathrm{LB}}, \\
P_0(k^*) &= (0,0)\,, \\
P_1(k^*) &= (0.8471436672437109\ldots, 1.691664920976177\ldots)\,, \\
V_0(k^*) &= (1.7675368645589482\ldots, 3.372726522382239\ldots)\,, \\
V_1(k^*) &= (1.9530111855752121\ldots, 0.094167780690677\ldots)\,.
\end{aligned}$$

This results in the following 2D crystal structure, see Fig. 1, which shows the unit cell and a piece of the crystal this generates. Note that we have confirmed that at least one the packings of Ref. [30] can be impoved upon by large scale reorganizations. Also note that this configuration forms a centrosymmetric-dimer lattice.

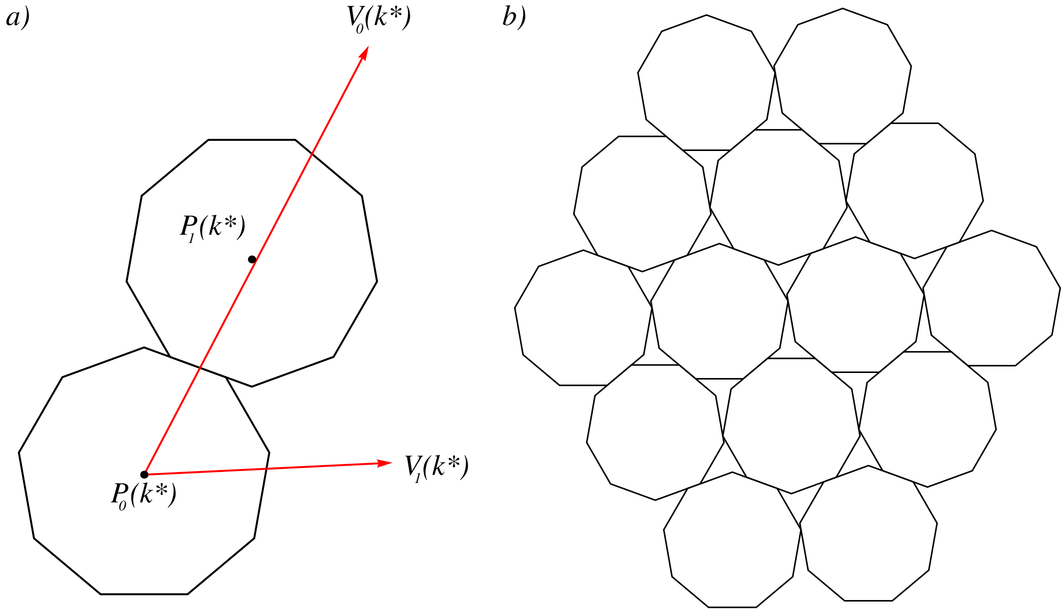


FIG. 1: **New densest-packing crystal structure for enneagons.** (a) The unit cell vectors $V_0(k^*)$ and $V_1(k^*)$ and the $N = 2$ enneagons in it, positioned at $P_0(k^*)$ and $P_1(k^*)$. (b) A piece of the crystal structure this dimer generates.

**Truncated tetrahedra:** For the system containing $N = 2$ truncated tetrahedra we provide additional information on the composition of the dimer lattice that we obtained using our method and which achieves a packing fraction $\phi_{\mathrm{LB}} = 0.988\ldots$. Table XIV lists the position and orientation of the particles within the unit cell, as well as the shape of the cell itself. We have transformed the unit cell of the dimer lattice ($N = 2$), using lattice reduction[4], in such a way that it is almost cubic and that one of the particles is located in the origin.

TABLE XIV: **Coordinates which specify the dimer lattice of truncated tetrahedra.** This Table lists the 12 vertices $\mathbf{v}$ of the truncated tetrahedron model used in our simulations. It also gives the three vectors $\mathbf{u}_m$, with $m = 1, 2, 3$ an index, which span the unit cell; the two position vectors $\mathbf{R}_i$, with $i = 1, 2$ the particle number, which indicate where the truncated tetrahedra are located with respect to the origin; and the two rotation matrices $\mathbf{M}_i$, which specify how to rotate the particles from their initial configuration. This initial configuration is given by the set of $\mathbf{v}$ presented here. A single vertex is a three dimensional (3D) vector, of which the components are indicated by $v_x$, $v_y$, and $v_z$, relative to a standard Cartesian coordinate frame. These $\mathbf{v}$ have been written in a row format in the Table, other vectors are treated similarly. The entries of the matrices $\mathbf{M}$ are denoted as $M_{kl}$, with $k$, $l = x, y, z$. For this choice of vertices, the volume enclosed by the particle's surface is unity. We have provided all vector and matrix entries in 6 decimal precision. Rounding errors may lead to small overlaps of particles in the crystal generated using these coordinates.

| $v_x$ | $v_y$ | $v_z$ | $v_x$ | $v_y$ | $v_z$ | | $u_x$, $R_x$ | $u_y$, $R_y$ | $u_z$, $R_z$ |
|---|---|---|---|---|---|---|---|---|---|
| 0.621121 | -0.358604 | -0.439200 | 0.621121 | 0.358604 | -0.439200 | $\mathbf{u}_1$ | 0.241977 | 0.928872 | 0.855892 |
| 0.828162 | 0.000000 | 0.146400 | -0.414081 | -0.717209 | 0.146400 | $\mathbf{u}_2$ | 0.604353 | -0.735843 | 0.832841 |
| -0.621121 | -0.358604 | -0.439200 | 0.000000 | -0.717209 | -0.439200 | $\mathbf{u}_3$ | -1.053988 | -0.200499 | 0.654313 |
| 0.000000 | 0.717209 | -0.439200 | -0.621121 | 0.358604 | -0.439200 | | | | |
| -0.414081 | 0.717209 | 0.146400 | -0.207040 | 0.358604 | 0.732000 | $\mathbf{R}_1$ | 0.000000 | 0.000000 | 0.000000 |
| -0.207040 | -0.358604 | 0.732000 | 0.414081 | 0.000000 | 0.732000 | $\mathbf{R}_2$ | -0.073508 | -0.001753 | 0.875316 |

| | $M_{xx}$ | $M_{xy}$ | $M_{xz}$ | $M_{yx}$ | $M_{yy}$ | $M_{yz}$ | $M_{zx}$ | $M_{zy}$ | $M_{zz}$ |
|---|---|---|---|---|---|---|---|---|---|
| $\mathbf{M}_1$ | -0.892816 | -0.442579 | 0.083685 | -0.443985 | 0.896032 | 0.001996 | -0.075867 | -0.035373 | -0.996490 |
| $\mathbf{M}_2$ | 0.892816 | -0.442579 | -0.083685 | 0.443985 | 0.896032 | -0.001996 | 0.075867 | -0.035373 | 0.996490 |

### Visual Representations of the Closest Packing Results

In this section we visually represent the data of Tables I - XI to show that there is no clear relation between the sphericity $\gamma$ and the densest packing fraction $\phi_{\mathrm{LB}}$ for the 159 particle species that we have investigated. Here, we also show that for the convex particles Ulam's conjecture is satisfied. Finally, we give more extensive visual representations of some of the data in Tables III, IX and X by showing several of the packings achieved using our method.

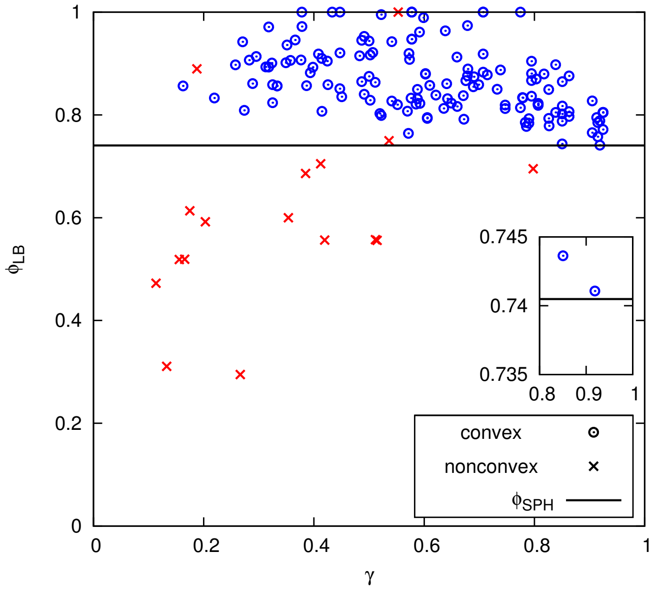


FIG. 2: **Packing fraction for the densest-known configuration of a particle and the relation to its sphericity.** The graph shows the achieved maximum packing fraction $\phi_{\mathrm{LB}}$ as a function of the sphericity $\gamma$ for the convex particles (circles, blue) and nonconvex particles (crosses, red) we investigated. Also see Tables I - XI for the numerical value associated with this data. Note that particles with a sphericity of $\gamma > 0.8$ tend to group closer to the packing fraction of spheres ($\phi_{\mathrm{SPH}}$, solid line). However, there is significant spread in the $\phi_{\mathrm{LB}}$ for all particles we considered, even for $\gamma > 0.8$. Therefore, we conclude that there is no clear relation between $\gamma$ and $\phi_{\mathrm{LB}}$ on the strength of our data. Using the line $\phi_{\mathrm{SPH}}$ and the inset, we show that all convex particles satisfy Ulam's conjecture.

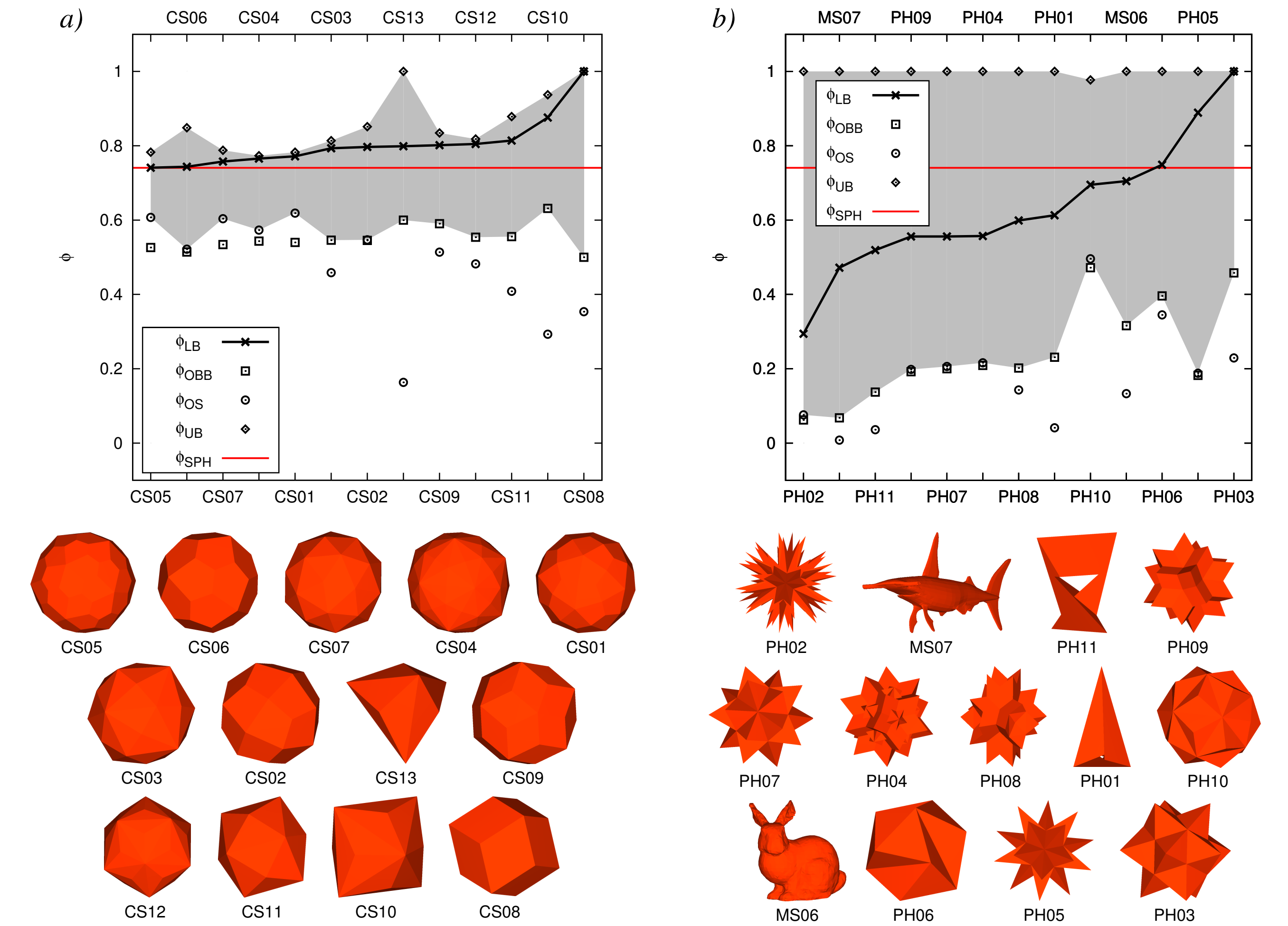


FIG. 3: **Upper and lower bounds to the densest packing fraction.** Graph (a) shows bounds to the densest packing fraction for 13 Catalan solids and graph (b) shows analogous data for 13 nonconvex solids. The graphs show the achieved densest-known packing fraction ($\phi_{\mathrm{LB}}$, connected crosses), as well as the outscribed-sphere lower bound ($\phi_{\mathrm{OS}}$, circles), oriented-bounding-box lower bound ($\phi_{\mathrm{OBB}}$, squares), and inscribed-sphere upper bound[7] ($\phi_{\mathrm{UB}}$, diamonds) values to the packing fraction for the models given below it. Also see Table III, IX and X, which gives both the numerical values and the full name corresponding to the abbreviations used here. Based on the available data we expect to find our FBMC result inside the gray area, which is bounded from below and above by the established lower and upper bound to the densest packing fraction respectively. The value of the densest packing for spheres $\phi_{\mathrm{SPH}}$ is indicated by a red line. Note that the improvement of the FBMC method with respect to the established lower bounds is significant for all models.

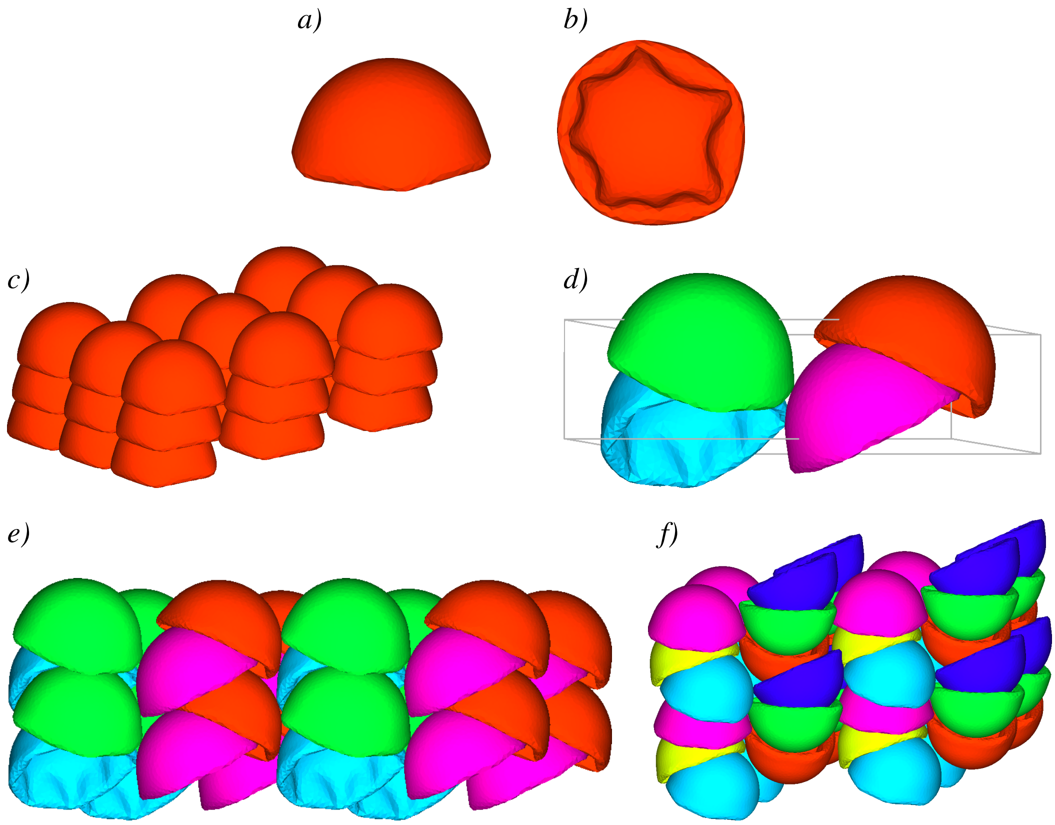


FIG. 4: **Several crystal structures achieved for a model of a colloidal cap.** This figure shows two views of the cap model used in our simulations (a) - (b), which is representative of colloidal caps obtained in syntheses, see for instance Refs. [37] and [38]. The cap model is derived from the numerical analysis of the collapse of a spherical shell. This analysis[35,39] was performed using Surface Evolver[40] to minimize the Hamiltonian, which describes the properties of the shell. The Hamiltonian incorporates bending and in-plane stretching elasticity terms to properly account for the physics behind the collapse under an external isotropic pressure. Note the buckling that has occurred in the impression left by the shell collapse (b). Also note that the model is not rotationally symmetric (b). We find several crystal-structure candidates. For $N = 1$ we find a columnar phase (c); the 26 of its periodic images are shown. For $N = 2$, 3, 4, and 5, we obtain braided phases without inversion, such phases are labeled 'B' in Ref. [41]. The unit cell and crystal structure for $N = 4$ particles in the unit cell are shown in (d) and (e) respectively, where we have labelled the different caps with colors. The structure is a binary braided configuration; only 7 periodic images are shown. The binary nature is likely due to the lack of rotational symmetry, which allows for better packing. Finally, for $N = 6$ we obtain a rough braided phase with inversions (f), which looks similar to the 'IB phase' predicted in Ref. [41]; again only 7 periodic images are shown and colors were used to aid in indentifying the periodicity. Because of the substantial difference in shape to the bowl-shaped particles used in Ref. [41], we do not think it appropriate to assign an approximate $L/\sigma$ (see Ref. [41]) value to the cap model.

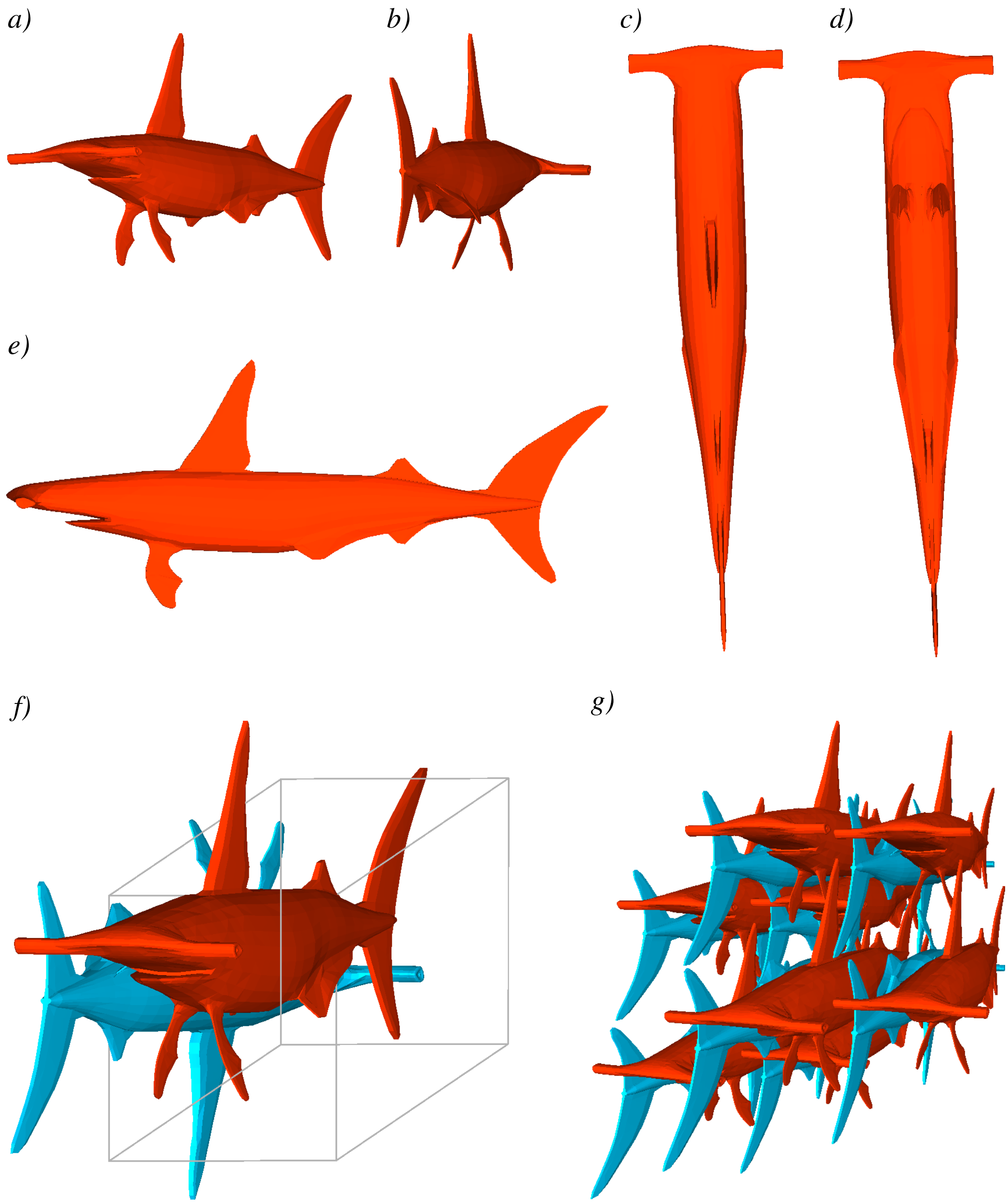


FIG. 5: **The densest known regular packing of hammerhead shark models.** Different views (a) - (e) of hammerhead shark model.[32] The unit cell of the densest regular packing ($\phi_{\rm LB} = 0.472$) is shown in (f), and a piece of the crystal in (g). The crystal structure is a double lattice where two hammerhead sharks (red, blue) point in opposite directions and one is rotated by an angle of $\sim \pi$ radians around its long axis with respect to the other, thereby forming a centrosymmetric dimer.

[*] Electronic address: j.degraaf1@uu.nl
[†] Electronic address: m.dijkstra1@uu.nl
[1] L. Filion et al., Phys. Rev. Lett. **103**, 188302 (2009).
[2] J. de Graaf, M. Dijkstra, and R. van Roij, Phys. Rev. E **80**, 051405 (2009).
[3] GAMMA Research Group at the University of North Carolina, RAPID - Robust and Accurate Polygon Interference Detection, http://gamma.cs.unc.edu/OBB/, 1997.
[4] D. Gottwald, G. Kahl, and C. N. Likos, J. Chem. Phys. **122**, 204503 (2005).
[5] E. R. Chen, M. Engel, and S. C. Glotzer, Discrete Comput. Geom. **44**, 253 (2010).
[6] U. Betke and M. Henk, Comput. Geom. **16**, 157 (2000).
[7] S. Torquato and Y. Jiao, Nature Lett. **460**, 876 (2009).
[8] S. Torquato and Y. Jiao, Phys. Rev. E **80**, 041104 (2009).
[9] S. Torquato and Y. Jiao, Phys. Rev. E **81**, 041310 (2010).
[10] S. Gottschalk, M. C. Lin, and D. Manocha, OBBTree: a hierarchical structure for rapid interference detection, in *Proceedings of the 23rd annual conference on Computer graphics and interactive techniques*, SIGGRAPH '96, page 171, Association for Computing Machinery (New York), 1996.
[11] G. Vernizzi, R. Sknepnek, and M. Olvera de la Cruz, Europ. J. Combinatorics **21**, 807 (2000).
[12] U. Agarwal and F. A. Escobedo, Nat. Mater. **10**, 230 (2011).
[13] A. Mews, A. V. Kadavanich, U. Banin, and A. P. Alivisatos, Phys. Rev. B **53**, R13242 (1996).
[14] E. C. Greyson, J. E. Barton, and T. W. Odom, Small **2**, 368 (2006).
[15] F. Kim et al., Angew. Chem. **116**, 3759 (2004).
[16] Y. Sun and Y. Xia, Science **298**, 2176 (2002).
[17] X. Zhang et al., Angew. Chem. **48**, 9121 (2009).
[18] H.-L. Wu, C.-H. Kuo, and M. H. Huang, Langmuir **26**, 12307 (2010).
[19] E. Matijevic, Acc. Chem. Res. **14**, 22 (1981).
[20] A. Tao, P. Sinsermsuksakul, and P. Yang, Angew. Chem. **45**, 4597 (2006).
[21] I. R. Fisher et al., Phys. Rev. B **59**, 308 (1999).
[22] K. Kwon et al., J. Phys. Chem. C **111**, 1161 (2007).
[23] J. Tang et al., J. Am. Chem. Soc. **129**, 9044 (2007).
[24] Y. Jiao and S. Torquato, Arxiv **1107.2300v3**, na (2011).
[25] P. F. Damasceno, M. Engel, and S. C. Glotzer, Arxiv **1109.1323v1**, na (2011).
[26] B. Wiley, T. Herricks, Y. Sun, and Y. Xia, Nano Lett. **4**, 1733 (2004).
[27] A. S. Barnard, X. M. Lin, and L. A. Curtiss, J. Phys. Chem. B **109**, 24465 (2005).
[28] Y. Saito, K. Mihama, and R. Uyeda, J. Cryst. Growth **45**, 501 (1978).
[29] Y. Saito, K. Mihama, and R. Uyeda, Jpn. J. Appl. Phys. **19**, 1603 (1980).
[30] Y. Limon Duparcmeur, A. Gervois, and J. P. Troadec, J. Phys. I France **5**, 1539 (1995).
[31] Stanford University Computer Graphics Laboratory, Stanford Bunny PLY-model, http://graphics.stanford.edu/data/3Dscanrep/, 1993.
[32] J. Burkardt, Hammerhead Shark PLY-model, http://people.sc.fsu.edu/~jburkardt/data/ply/ply.html, 1993.
[33] Wolfram Research, Inc., Mathematica 1, Software Package, 1988.
[34] Wolfram Research, Inc., Mathematica 7, Software Package, 2009.
[35] C. Quilliet et al., Eur. Phys. J. E **27**, 13 (2008).
[36] T. C. Hales and S. P. Ferguson, Discete Comput. Geom. **36**, 1 (2006).
[37] C. I. Zoldesi and A. Imhof, Adv. Mater. **17**, 924 (2005).
[38] D. Jagadeesan et al., Angew. Chem. **47**, 7685 (2008).
[39] N. Tsapis et al., Phys. Rev. Lett. **94**, 018302 (2005).
[40] K. Brakke, Exp. Math. **1**, 141 (1992).
[41] M. Marechal et al., Nano Lett. **10**, 1907 (2010).